

CFD Project

Harsharaj Birendrasingh Parmar

Flow around a square cylinder

1 Introduction

External flows play a critical role in examining practical fluid flow phenomena with a notable one being the periodic shedding of vortices about a long cylindrical structure. This shedding creates a street of alternate vortices in the wake of the body termed as the Von-Karman vortex street. Numerous practical structures fit into this description like skyscrapers, long spanned bridges, transmission wires and others. The vortices cause periodic forcing on the structure leading to vibrations and flow induced acoustics which need to be examined for design purposes. The present work considers 2D flow around a square cylinder using the Immersed boundary method which can then be extended to model flows around arbitrary cross-sections. Three flow regimes are considered in the analysis namely Stokes flow, low-Re and high-Re transient Navier-Stokes equation. A primitive variable formulation is devised using a second order mixed explicit/implicit time integration scheme with Crank-Nicolson scheme operating on the diffusive terms and a second order Adams-Bashforth scheme acting on the convective terms. Second order spatial discretization is used for the derivatives and projection method is implemented to treat the velocity pressure coupling.

2 Problem Description

The problem represents two-dimensional flow over an infinitely long square cylinder with uniform free-stream velocity at the inlet, top and bottom boundaries of the system as shown in Fig 1.

The square cylinder has a length $L = 1$ and the computational domain has a length $L_c = 10$, width $W_c = 5$ to ensure that the conditions at the boundaries do not affect the physics near the cylinder. The Reynolds number is varied from 0.01 to 1000 and the domain is divided into 100 elements lengthwise and 50 elements along the width. A transient solution technique is adopted with a time step 10^{-3} to ensure stability.

Flow is assumed to be incompressible and body forces are assumed to be absent in the analysis.

Spatial Discretization

The spatial discretization is carried out using Finite Difference approximations of the derivatives. Second order accurate approximations are defined at every point in the domain. At the boundaries, one sided second order approximations for the first and second order

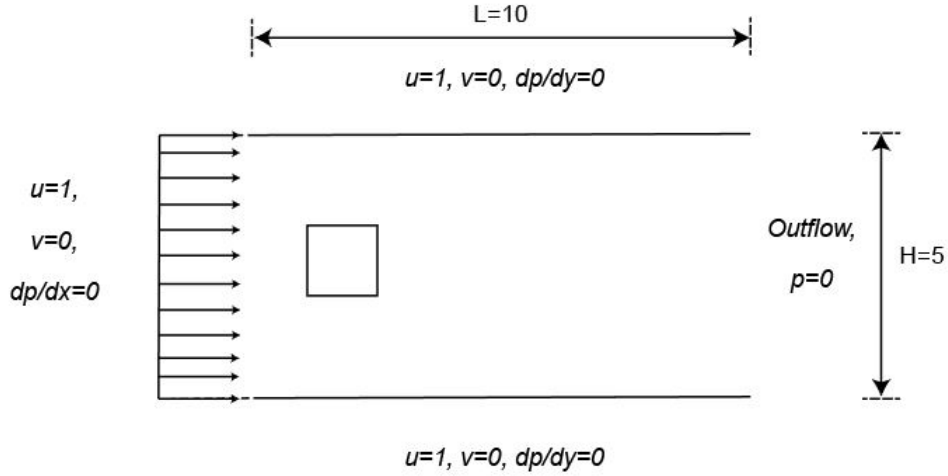


Figure 1: Physical domain

derivatives are defined. In the interior of the domain, central differencing is done for the first and second order derivatives.

At the boundaries,

$$\frac{\partial u}{\partial x_i} = \frac{3u_i - 4u_{i-1} + u_{i-2}}{2\Delta x} \quad \text{or} \quad \frac{\partial u}{\partial x_i} = \frac{-3u_i + 4u_{i+1} - u_{i+2}}{2\Delta x}$$

$$\frac{\partial^2 u}{\partial x^2_i} = \frac{2u_i - 5u_{i-1} + 4u_{i-2} - u_{i-3}}{\Delta x^2} \quad \text{or} \quad \frac{\partial^2 u}{\partial x^2_i} = \frac{2u_i - 5u_{i+1} + 4u_{i+2} - u_{i+3}}{\Delta x^2}$$

In the interior,

$$\frac{\partial u}{\partial x_i} = \frac{u_{i+1} + u_{i-1}}{2\Delta x} \quad \frac{\partial^2 u}{\partial x^2_i} = \frac{u_{i+1} - 2u_i + u_{i-1}}{\Delta x^2}$$

Note that in the above expressions the j index is not changing and so has been omitted for clarity. Similarly we can define the derivatives in the y -direction for the point (i, j) and form the derivative matrices required for our computations. One-sided approximations work for finding the derivative values at the boundaries when the velocity has already been solved and known. But while enforcing Neumann boundary conditions they need to be changed in order to increase computational efficiency as we shall see later.

Temporal Discretization

Temporal discretization is carried out using a second-order semi-implicit time integration scheme [1]. The time integration scheme is formed as a combination of Crank-Nicolson scheme acting on the diffusive terms and Adams-Bashforth scheme acting on the convective terms. Combination of an explicit second-order Adams-Bashforth scheme for the advection terms and an implicit Crank-Nicolson scheme for diffusion terms can be described as follows:

$$NL(\phi) = \frac{3}{2}NL(\phi^n) - \frac{1}{2}NL(\phi^{n-1})$$

$$D(\phi) = \frac{D(\phi) + D(\phi^n)}{2}$$

where $NL(\phi)$ and $D(\phi)$ represent,

$$NL(\phi) = u \frac{\partial \phi}{\partial x} + v \frac{\partial \phi}{\partial y} \quad D(\phi) = \frac{\partial^2 \phi}{\partial x^2} + \frac{\partial^2 \phi}{\partial y^2}$$

Projection Method

Projection method belongs to the predictor-corrector class of algorithms and is non-iterative in nature. Pressure acts as a projection of the predicted velocity field to form a divergence free space in this class of methods.

- a) Advection-Diffusion step which involves the intermediate velocity at $(n + 1)\Delta t$, \tilde{V}

$$\frac{\tilde{V} - V^n}{\Delta t} = \frac{1}{Re} D(V) - NL(V) \quad in \quad \Omega$$

Here $NL(V) = (V \cdot \nabla)V$ and $D(V) = \nabla^2 V$ represent the advection and diffusion terms.

- b) Pressure correction step solves the Poisson equation for P^{n+1}

$$\nabla^2 P^{n+1} = \frac{\nabla \cdot \tilde{V}}{\Delta t} \quad in \quad \Omega$$

With homogeneous Neumann boundary conditions

$$\hat{n} \cdot \nabla P^{n+1} = 0 \quad on \quad \partial\Omega$$

Thereafter the velocities are updated as given below,

$$V^{n+1} = \tilde{V} - \Delta t \nabla P^{n+1} \quad in \quad \Omega + \partial\Omega$$

The solution then proceeds to the next time step where the entire method is repeated using the updated velocities. Here Ω represents the interior of the computational domain and $\partial\Omega$ represents the boundary of the domain.

Boundary Conditions

Velocity boundary conditions are straightforward for the inlet, top and bottom boundaries where the values of u, v components are provided and are 1, 0 respectively at each of the boundaries. At the outlet, open boundary conditions are implemented for both u, v so that they do not constrain the solution in any way. Outflow boundary conditions for a general variable ϕ are given as,

$$\frac{\partial\phi}{\partial t} + u_{av} \frac{\partial\phi}{\partial x} = 0$$

At the inlet, top and bottom boundaries,

$$u = 1 \quad \text{and} \quad v = 0$$

In our case, $u_{av} = 1$ and the x-derivative represents the normal to the outlet surface.

Pressure boundary conditions are set to Neumann type at the inlet, top and bottom boundaries where the normal derivatives of pressure are set to 0. At the outlet, a dirichlet boundary condition is implemented to maintain well-posedness of the problem and pressure value is set to 0.

$$p_{outlet} = 0$$

At the inlet, top and bottom boundaries (ghost nodes implemented for the top and bottom boundaries),

$$\frac{\partial p}{\partial n} = 0$$

If we use one-sided derivative approximations at the top and bottom boundaries then the bandwidth of the pressure coefficient matrix becomes twice and significantly hampers the computational speed of the algorithm. Thus ghost noding is done for pressure boundary conditions at the top and bottom boundaries which reduces the bandwidth, preserves the symmetry and provides significant speed-up.

Finally, the effects of the square cylinder are realized in the flow phenomena using the Immersed boundary method by forcing the velocity in the \tilde{V} calculation to be 0 on and within the solid body [2]. Rest of the procedure remains intact with the global velocity being used to find the pressure and subsequent known terms on the RHS of \tilde{V} .

$$\tilde{V} = 0 \quad \text{in} \quad \text{solid}$$

3 Results

The numerical formulation was run for various ranges of Re to encompass the different regimes and the post processing was done by exporting a .dat file to Tecplot. Firstly, very

low Re cases were examined to see the solution to the Stokes problem which is valid for $Re \ll 1$ and is commonly referred to as creeping flow. For the case of creeping flow we have a steady state solution to the problem where the streamlines seem to follow the solid body without the onset of separation. In Fig 2 the key point is to note that the streamlines follow the surface of the square throughout without any separation.

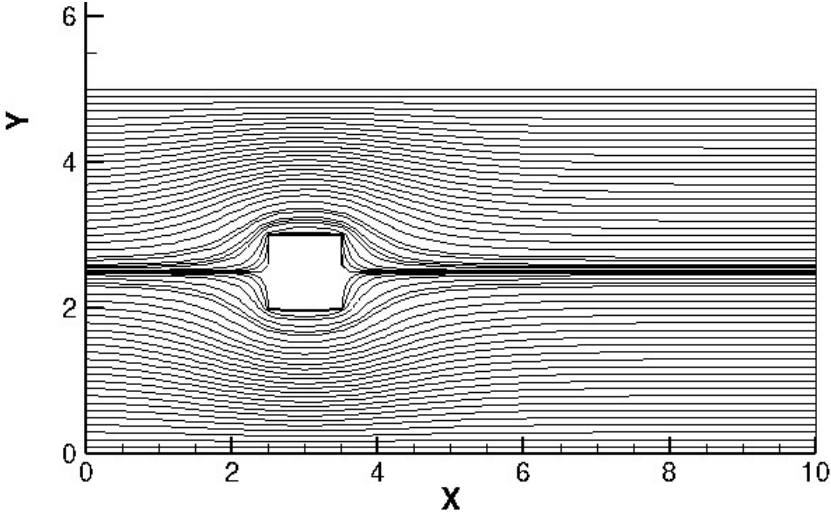


Figure 2: Streamlines plot in the Stokes regime

As we move to $Re = 1$ the symmetrical flow around the square starts stretching ever so slightly as shown in Fig 3.

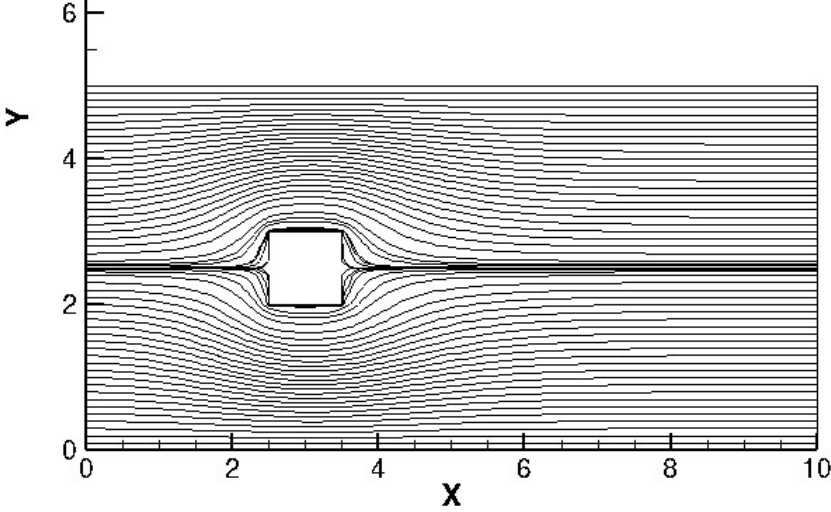


Figure 3: Streamlines plot at $Re = 1$

At $Re = 10, 100$ we observe the formation of stagnant vortices in the wake of the square and marks the first instance of recirculation being observed in our physics as shown in Fig 4 and 5

Next, the formulation was run at $Re = 1000$ and the plot of vorticity and velocity vectors

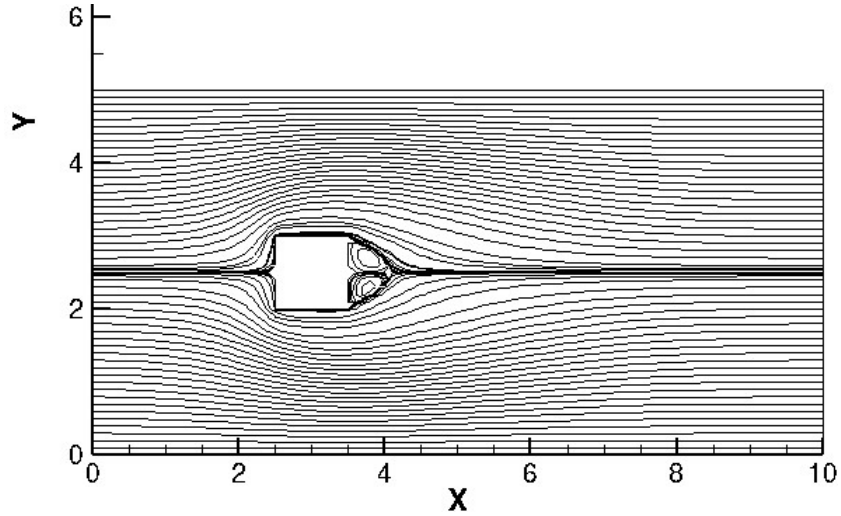


Figure 4: Streamlines plot at $Re = 10$

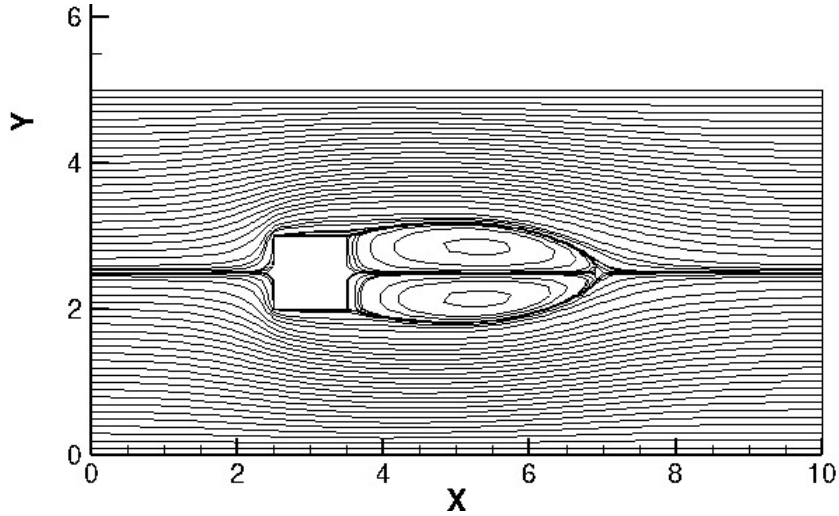


Figure 5: Streamlines plot at $Re = 100$

were observed over an extended period of time as shown in Fig 6.

The evolution of vortices is very slow for the uniform flow case and shedding occurs after a very long time even at this high Re . So in order to visualize the shedding an external shear was imposed in the inlet velocity boundary condition and then the contours were plotted with time to observe the shedding as shown in Fig 7, 8 and 9 [3]. Inlet velocity is changed to the following relation:

$$u_{in} = 1 + Ky$$

Finally, the values of velocity components were plotted at the mid point of the domain with the number of time steps to confirm the transient nature of the phenomena and the plots are shown in Fig 10 and 11.

4 Conclusions

A project method based second order accurate (both spatial and temporal) finite difference scheme is developed in this work to solve fundamental fluid flow phenomena. This scheme was validated by performing a channel flow test wherein the exact solution can be determined analytically and compared with the numerical results. Furthermore, Immersed Boundary Method is used in conjunction to model laminar flow past an infinitely long square cylinder. Efforts have been made to establish the formulation for simple geometries initially which can then be extended to complicated solid bodies as per the problem's demands.

Three regimes were considered for modelling the flow past a cylinder and the results obtained were in accordance to expectations and qualitatively validated by prevalent results in literature. Stokes flow condition was implemented and the symmetrical distribution of the streamlines was observed which validated results from that regime. For low Re stagnant vortices are formed in the wake of the cylinder which is expected below the critical Re required for shedding to start. Finally, high Re solutions were carried out to observe the alternate shedding of vortices or the Von-Karman vortex street providing evidence of the ability to handle instabilities and full blown transient integration of the physics by the implemented scheme.

No claims have been made endorsing the current scheme to be superior or in comparison to benchmark results and in a way the validation is largely void due to the lack of quantitative comparisons like C_{lift} , C_{drag} , St and others. But we can surely claim that the current scheme is able to capture the physics of the problem over a wide range of Re with acceptable accuracy and stability which serves for basic computations.

References

- [1] J. J. Martinez and P. T. Esperana. *A Chebyshev collocation spectral method for numerical simulation of incompressible flow problems*. Journal of the Brazilian Society of Mechanical Sciences and Engineering, 29(3), 2007, 317-328.
- [2] Piyush K. Kundu, Ira M. Cohen. *Fluid Mechanics*. Academic Press; 6 edition (June 19, 2015).
- [3] M. Cheng, D. S. Whyte, J. Lou. *Numerical simulation of flow around a square cylinder in uniform-shear flow*. Journal of Fluids and Structures, Volume 23, Issue 2, February 2007, Pages 207-226

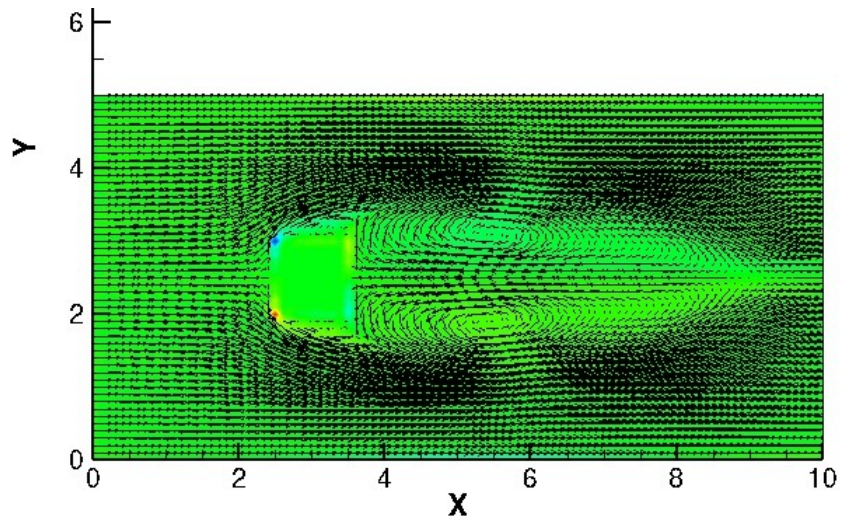
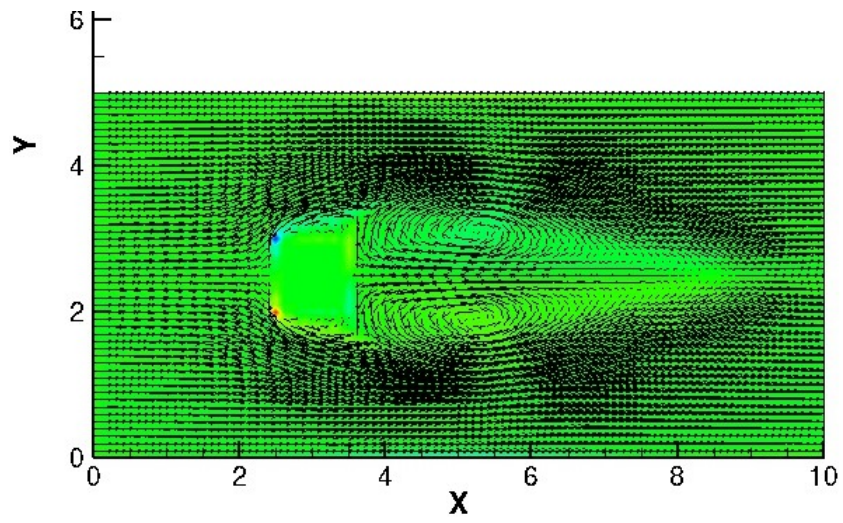
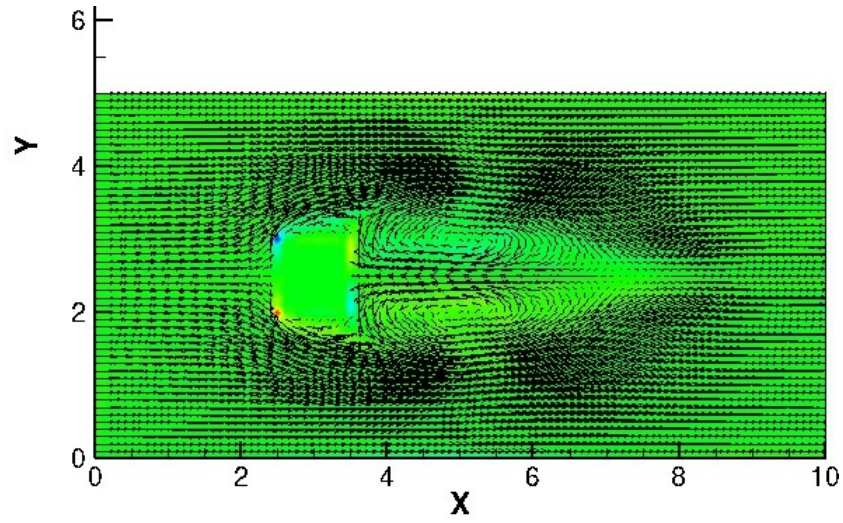


Figure 6: Comparison of vorticity contours and velocity vectors at $t = 12, 16$ and 22 sec

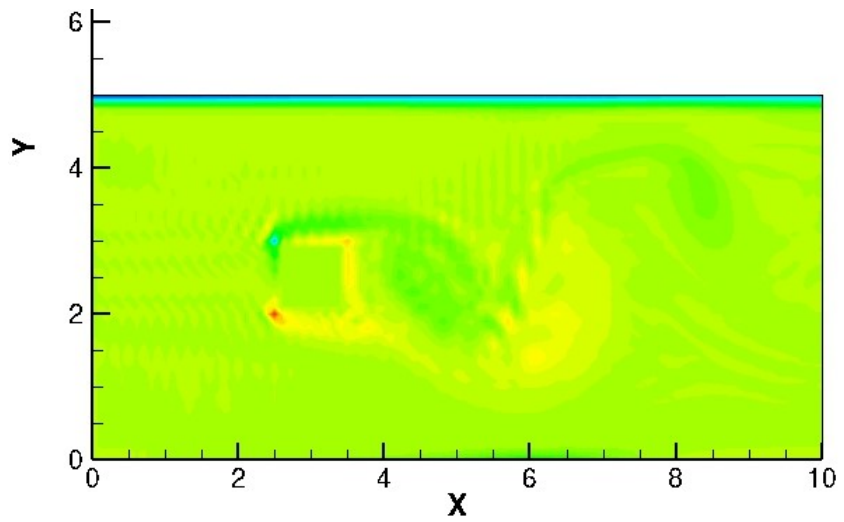
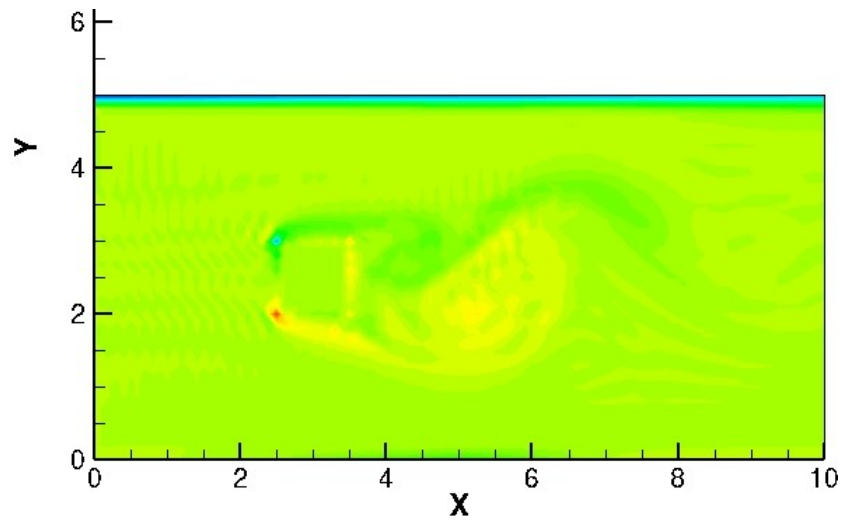
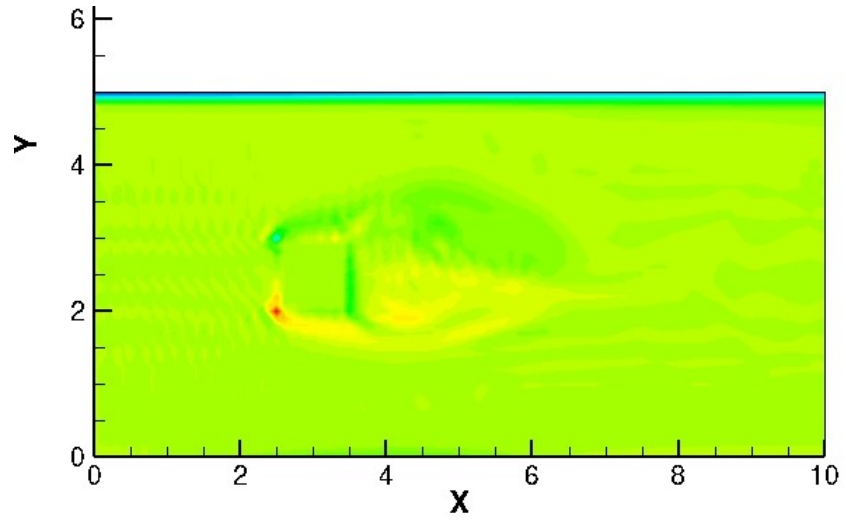


Figure 7: Time evolution of vorticity contours at $Re = 1000$

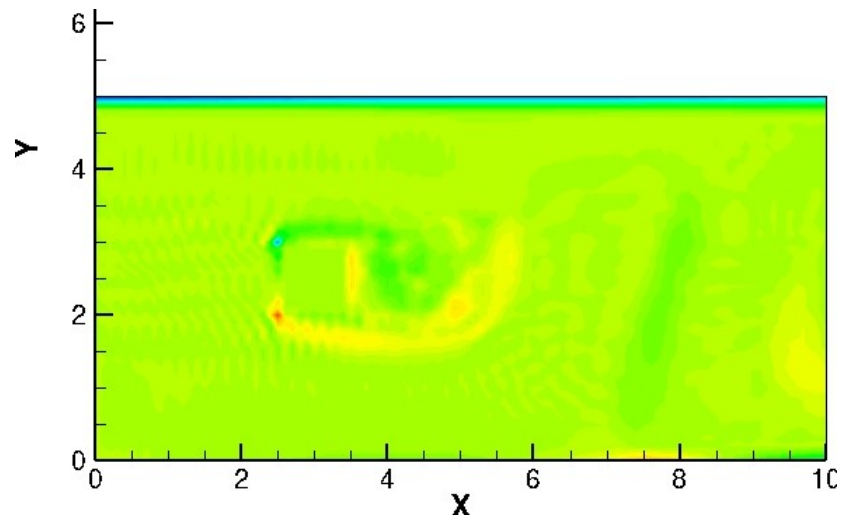
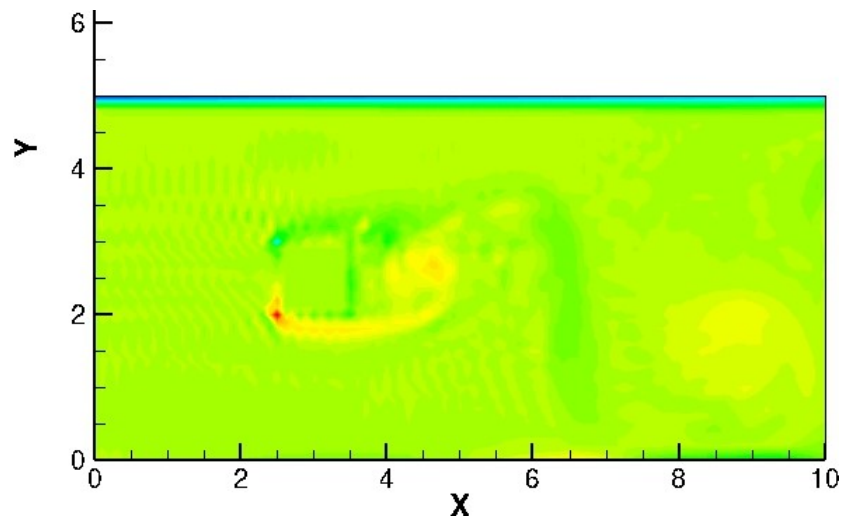
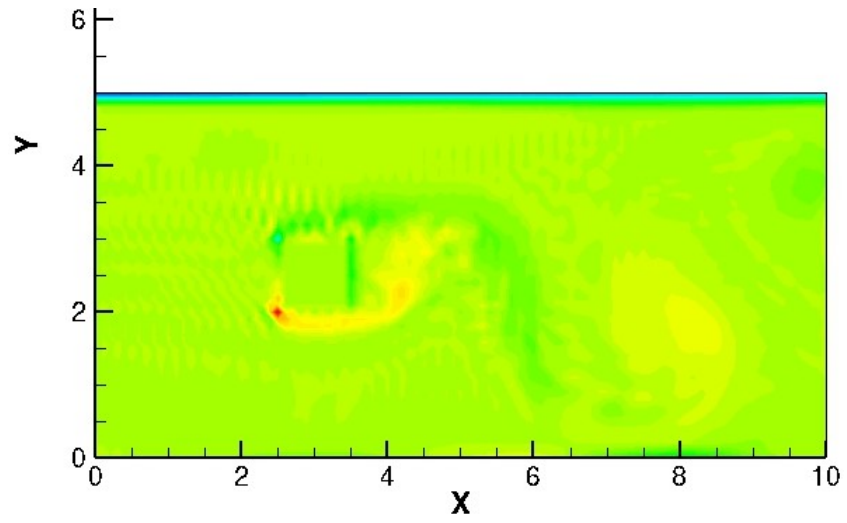


Figure 8: Time evolution of vorticity contours at $Re = 1000$ (continued)

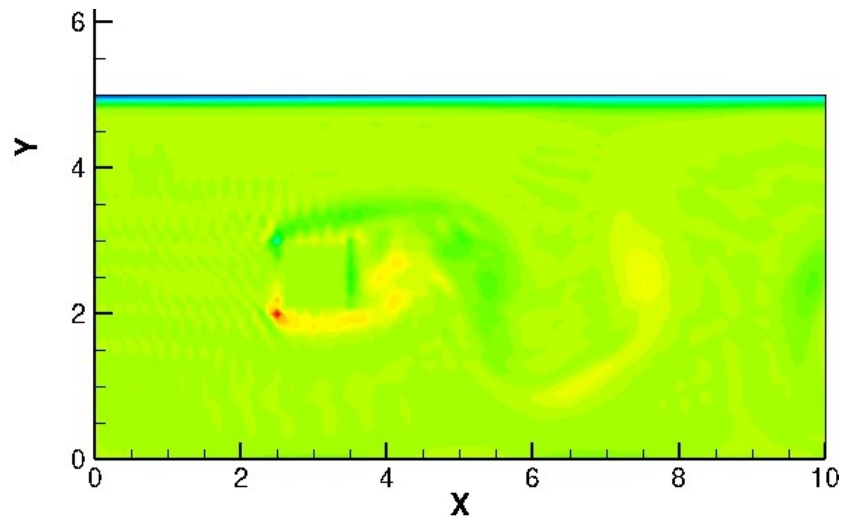
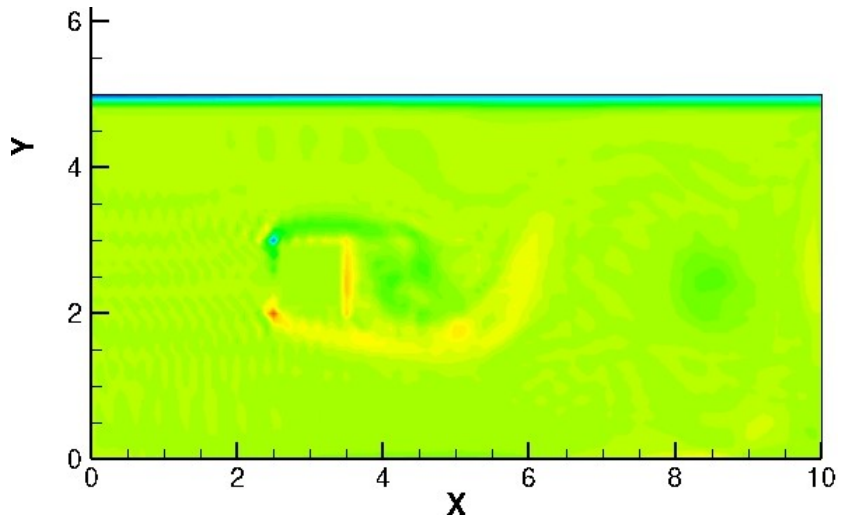
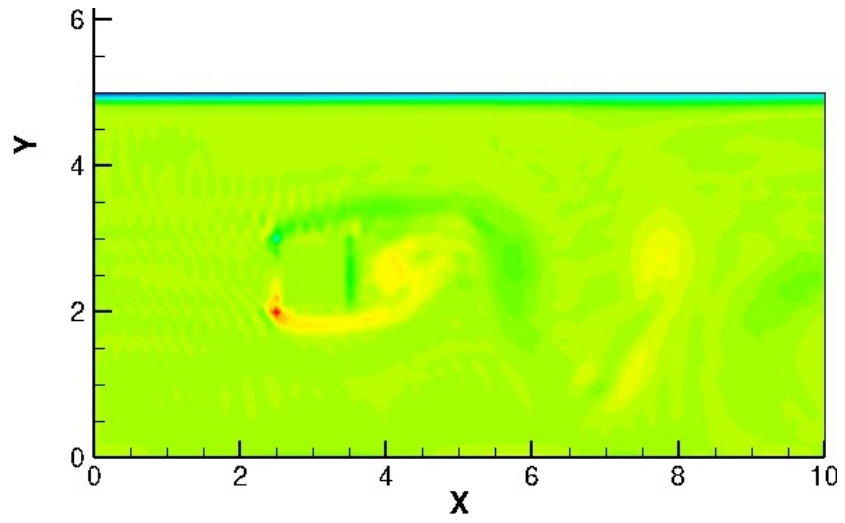


Figure 9: Time evolution of vorticity contours at $Re = 1000$ (continued)

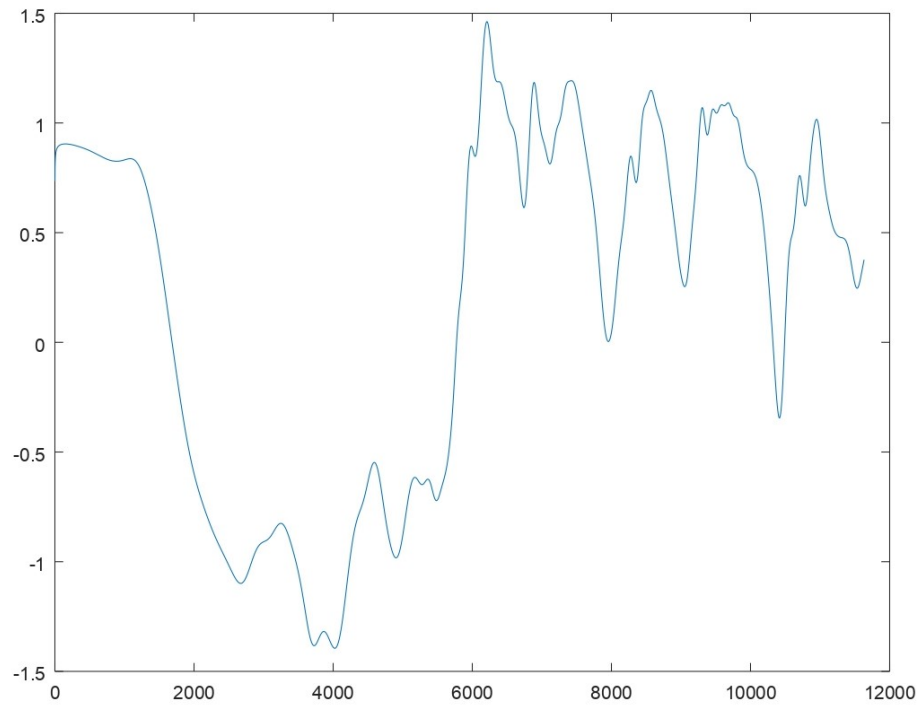


Figure 10: Mid-point values for u with time steps

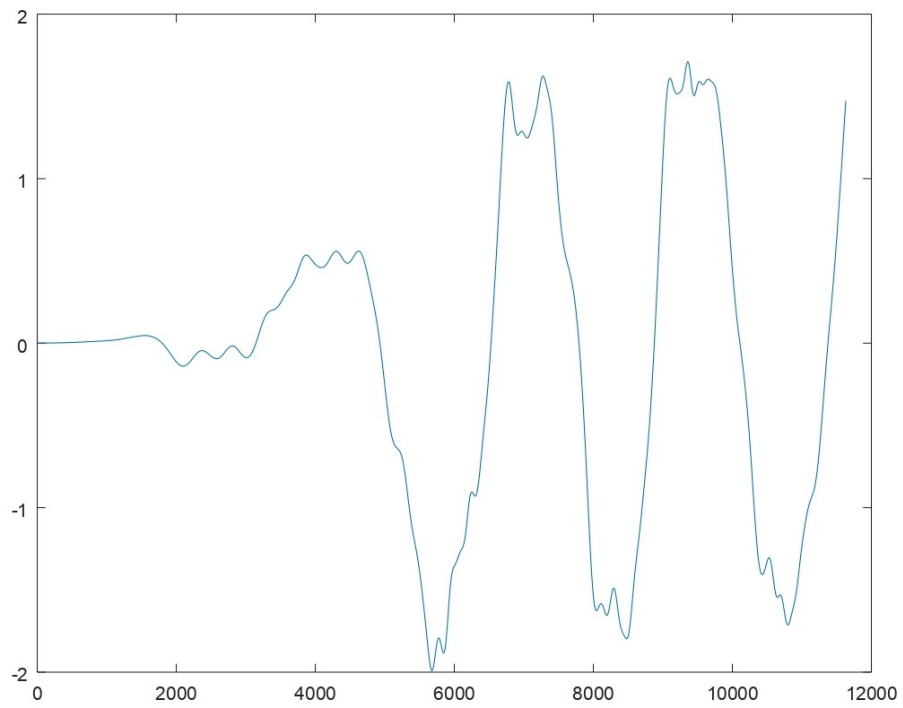


Figure 11: Mid-point values for v with time steps